Journal of Rehabilitation in Civil Engineering 9-4 (2021) 148-170

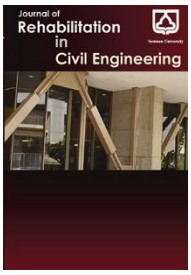

journal homepage: http://civiljournal.semnan.ac.ir/

Shear and Flexural Strengthening of Steel Beams with Thick Carbon Fiber Reinforced Polymer Laminate

Mohammad Shekarchi[1], Alireza Khaloo[2*]

1. Department of Civil Engineering, Sharif University of Technology, Tehran, Iran
Corresponding author: *khaloo@sharif.edu*

ARTICLE INFO

Article history:
Received: 09 January 2021
Revised: 17 May 2021
Accepted: 26 June 2021

Keywords:
Flexural behavior;
Shear behavior;
Lateral torsional buckling;
3-Point bending test;
CFRP laminate.

ABSTRACT

In this paper, shear and flexural behavior of structural steel beams strengthened by high modulus carbon fiber reinforced polymer (CFRP) laminates are presented. Totally, 18 steel specimens including 6 un-strengthened beams as control specimens and 12 strengthened steel beams with simple supports were tested under 3-point bending test set-up. All specimens were strengthened using the bonded system. Influence of different parameters including length of steel beams, section size of specimens, number of CFRP laminates, and location of CFRP laminates were studied. Based on anticipated failure modes, the bonded laminates were implemented on the surface of tension flange, compression flange, and web of beams. Three failure modes of flexural, shear, and lateral-torsional buckling failures were observed in the tested beams. The main goal of these experiments was to evaluate the enhancement in load capacity, beam ductility, and initial stiffness. The results showed that the yield load, ultimate load capacity, and energy absorption of strengthened steel beams improved up to 15, 29 and 28 percent, respectively. Finally, in order to predict test results and compare the actual and predicted valves, analytical and numerical studies were carried out.

1. Introduction

In many countries, there are some steel structures, in particular, steel beams, which either have lost their serviceability or are losing it and are in need of strengthening to gain demanded strength. These deficiencies can be due to undesirable design, wrong implementation, bad maintenance, fatigue damages, corrosion, degradations, and even

How to cite this article:
Shekarchi, M., Khaloo, A. (2021). Shear and flexural strengthening of steel beams with thick carbon fiber reinforced polymer laminate. Journal of Rehabilitation in Civil Engineering, 9(4), 148-170.
https://doi.org/10.22075/JRCE.2021.22339.1473

changes in design codes. In rudimentary techniques, these unsuitable steel beams were strengthened by attaching some additional steel plates to major surfaces of initial members. In these techniques, the steel plates and the structural steel member would be linked together by using bolts or welding. However, this can lead to increase the need of equipment and competent human resources to attach steel plates on its proper places, increase in project time, increase the weight of existing member and consequently the weight of entire structure and the low flexibility of steel plates in order to rehabilitate different shape of members [1, 2]. Moreover, the temperature of existing and additional members will be raised by welding these two parts to link together. Therefore, the structure experiences excess stresses as thermal stress and this aspect must be considered in designing them. Many studies have been conducted in order to retrofit and improve the behavior of concrete and timber members [3-10], but there is a requirement to focus on rehabilitating the flexural and shear behavior of steel beams using CFRP laminates.

Due to the fact that CFRP laminates are high-strength material, the bond stress plays an important role in strengthening. Teng et al. [11] and Al-Mosawe et al. [12] indicated that the selection of proper adhesive is necessary for bearing the bond stress well. Two factors of short-term mechanical performance and long-term durability of adhesive were considered by them. They also showed that for strengthening steel structural members, CFRP sheets or strips can show a better performance in comparison to other types of fiber-reinforced polymer (FRP) sheets like glass FRPs since CFRP laminates have higher stiffness. Madhavan et al. [13] conducted an experimental study on strengthening structural steel angle section using CFRPs. They revealed that not only do CFRPs increase load-carrying capacity of simple steel beams, but also it can improve the stiffness of specimens. In addition, it was revealed that the orientation of fiber reinforcement has a significant influence on the strength of retrofitted beams. Three large-scale concrete-steel composite beam girders strengthened by CFRP plates were tested and evaluated by Tavakkolizadeh and Saadatmanesh [14]. The results revealed that the ultimate load capacity of strengthened beams improved. Moreover, it was shown that with more number of CFRP layers, there is less efficiency of CFRP sheets. To simulate the damaged steel beams in bridges, Al-saidy et al. [15] deteriorated deliberately the specimens and rehabilitated them with CFRP plates adhered to tension flanges of composite beams. Their results indicate a remarkable improvement in ultimate load carrying capacity and stiffness of reinforced beams. All the specimens also were fully restored to their undamaged ultimate strength and stiffness. Hmidan et al. [16] conducted an experimental study to figure out the interaction between the magnitude of an intentionally notched beam as a damaged beam and CFRP layers. They damaged different beams with various notch depths and different beam heights. Experimental results revealed that the level of damage could not affect the failure mode of retrofitted beams. Linghoff et al. [17] and Martinelli et al. [18] tested some steel specimens strengthened by CFRP strips. An analytical model was provided to predict the load-deflection behavior. The results manifested that the moment capacity of strengthened beams can be increased by attaching CFRP strips to the tension flange of steel beams. El Damatty et al. [19]

accomplished experimental and analytical study to evaluate the effect of Glass fiber-reinforced polymer (GFRP) sheets on improving the bending behavior of steel beams. The results showed that the ultimate moment capacity, yield moment capacity and initial stiffness of retrofitted beams were incremented about 78, 23 and 15 percent, respectively. The behavior of rolled steel beams strengthened with partial-length CFRP plates were evaluated by Lenwari et al. [20]. The results pointed out that there were two failure modes in specimens: (1) plate debonding (2) plate rupture, according to the length of plates used in beams. Also, they reported that a noticeable improvement was observed in the moment-curvature and the load-deflection of strengthened beams. Rizkalla et al. [21] conducted experimental studies on various strengthening approaches of concrete-steel composite beams of bridges using different CFRP modulus and pre-stressed CFRP strips. They found out that the elastic and initial stiffness of repaired beams could increase between 10 and 34 percent, and the ultimate load-carrying capacity of specimens can be increased about 46 percent. Furthermore, the results approved the effectiveness of using pre-stressed CFRP in strengthening damaged bridge composite beams. Ghafoori et al. [22] studied the fatigue behavior of notched beams retrofitted by pre-stressed and non-prestressed CFRP plates under cyclic load, experimentally. The results showed that the pre-stressing of CFRP plates could increase the fatigue life of repaired beams by more than five times of non-prestressing repaired beams. Moreover, the results indicated that residual deflection during the fatigue crack growth process could be remarkably diminished by pre-stressing of CFRP plates. Ghafoori and Motavalli [23, 24] evaluated the effectiveness of using prestressed un-bonded CFRP plates for strengthening steel beam. They concluded that using un-bonded CFRP could improve the ultimate load capacity of beams. Also, this method was consuming less time since there was no need for application of adhesive and surface preparation of beams [25].

The in-plane bending behavior of steel beams retrofitted by CFRP layers has been previously investigated. The lateral-torsional buckling and shear failure are other two main failures which can occur during loading of steel beams. There are limited studies focusing on the strengthening steel beams against lateral-torsional buckling, all of which evaluated the effect of CFRP layers applied to the tension surface of beams. Also, to the authors' knowledge, no study has been reported to assess the effect of CFRP plate on the shear strength of steel beams.

In this paper, eighteen steel beams were tested with different lengths and CFRP strengthening configurations. By attaching CFRPs to the top flange, bottom flange, and web of beams, the stress level at steel beam is reduced because the CFRP carries a part of stresses. The goal of these experiments was to study the in-plane bending behavior of strengthened steel beams with various CFRP arrangements, the lateral buckling strength of steel beams retrofitted by an innovative method, and the advantages and disadvantages of applying unidirectional CFRP plates in order to improve the shear strength of steel beams. Besides, analytical and numerical models were developed to predict the behavior of specimens.

2. The experimental program

The objective of this experimental study is to assess flexural and shear behavior of steel

beams strengthened by CFRP laminates which are attached to flanges or web of steel beams. Furthermore, un-strengthened beams are considered as control specimens for each of the main failure modes including flexural, shear, and lateral-torsional buckling failures. The labeling of the steel beams and the types of strengthening are presented in Table 1.

Table 1. Experimental program.

Failure mode	Specimens number	Number of CFRP layers	Type of strengthening				Length [mm]	Designation*
			Top flange	Bottom flange	Right side of web	Left side of web		
flexural	1	-	-	-	-	-	500	F-IPE80-C
	2	1	-	✓	-	-	500	F-IPE80-B
	3	2	✓	✓	-	-	500	F-IPE80-TB
	4	2	-	✓✓	-	-	500	F-IPE80-BB
	5	-	-	-	-	-	500	F-IPE100-C
	6	1	-	✓	-	-	500	F-IPE100-B
	7	2	✓	✓	-	-	500	F-IPE100-TB
	8	2	-	✓✓	-	-	500	F-IPE100-BB
shear	9	-	-	-	-	-	200	S-IPE80-C
	10	1	-	-	✓	-	200	S-IPE80-R
	11	2	-	-	✓	✓	200	S-IPE80-RL
	12	-	-	-	-	-	200	S-IPE100-C
	13	1	-	-	✓	-	200	S-IPE100-R
	14	2	-	-	✓	✓	200	S-IPE100-RL
lateral-torsional buckling	15	-	-	-	-	-	1000	LT-IPE80-C
	16	1	✓	-	-	-	1000	LT-IPE80-T
	17	-	-	-	-	-	1000	LT-IPE100-C
	18	1	✓	-	-	-	1000	LT-IPE100-T

* Labeling include F, S and L as flexural, shear and lateral-torsional buckling, respectively. IPE stands for steel I section with 80 mm and 100 mm depth. C, B and T indicate control, bottom flange and top flange, respectively. R and L represent right and left side of web, respectively.

2.1. Materials

In order to strengthen the steel beams, CFRP laminates (Quantom® Carbon Plate® M1014) are used. The cross-sectional dimensions of composite laminates were 50 to 55 mm in width by 1.4 mm in thickness. The mechanical properties of the unidirectional CFRP laminates, reported by the manufacturer [26], are presented in Table 2 in accordance with ACI 440.3R-04 [27].

Table 2. Mechanical properties of the CFRP laminates.

Description	Value
Weave	unidirectional
Tensile strength [MPa]	≥2900 *
Young's modulus [GPa]	≥200 *
Poisson's ratio [-]	0.3
Elongation at break [%]	1.35

*For analytical and numerical calculations, the values of tensile strength and young's modulus are considered equal to 2900 MPa and 200 GPa, respectively.

The epoxy adhesive material includes two components for attaching the carbon laminates to the flange and web of steel beams. To have a better workability, one part of component B (hardener) was mixed with three parts of component A (resin) by weight. The pot life of this epoxy was 60 minutes and the epoxy was cured at 25 degrees of Celsius. The mechanical properties of the adhesive, as given by the manufacturer [28], are presented in Table 3.

Table 3. Mechanical properties of the adhesive.

description	Value
Tensile strength [MPa]	30
Shear strength [MPa]	20
Elongation at break [%]	1
Density (at 25 ºC)	1.65 kg/mixed liter
Full Cured	after 7 days (at 25 ºC)
Working Time / Pot Life	60 min. (at 25 ºC)
Color	concrete grey (mixed)

Two types of hot rolled sections, namely IPE80 and IPE100 were tested. The IPE profile was chosen due to the fact that the flexural stiffness along their strong axis was much higher than the other profiles such as HEA. In other words, the IPE section has a significantly higher principal flexural stiffness ratio ($(EI_x)/(EI_y)$) than the HEA profile. This property is important for specimens in which the lateral-torsional buckling is the investigated failure mode. Also, these IPE profiles are doubly symmetric I-shaped sections in which flanges and web are compact, so the occurrence of local buckling is prevented. The section properties of IPE80 and IPE100 are given in Table 4.

Table 4. Section properties of specimens.

section name	height of web(mm)	width of flange(mm)	thickness of web(mm)	thickness of flange(mm)	moment of inertia along x-axis (mm^4)	radius of gyration along x-axis (mm)	moment of inertia along y-axis (mm^4)	radius of gyration along y-axis (mm)
IPE80	80	47	3.8	5.2	801000	32.4	84900	10.5
IPE100	100	55	4.1	5.7	1710000	40.7	159000	12.4

To find out the mechanical properties of steel material used in beams, three samples were taken from the web of the steel beams by Computer Numerical Control (CNC) cutter machine, based on ASTM-E8 [29]. The tension specimen dimensions and shape are shown in Table 5 and Fig. 1, respectively. Based on the uniaxial tension test, the modulus of elasticity and the yield strength of steel are 200 GPa and 240 MPa, respectively.

Fig. 1. Steel tension sample.

Table 5. Specimen dimensions of steel tension sample.

Nominal width	value
Gage length [mm]	25
Width [mm]	6
Thickness [mm]	3.5
Radius of fillet [mm]	6
Overall length [mm]	100
Length of reduced section [mm]	32
Length of grip section [mm]	30
Width of grip section [mm]	10

2.2. Beam specimens preparation

According to the properties of the sections, steel beams were designed and cut into 200 mm, 500 mm and 1000 mm length pieces (support to support), due to the fact that the steel beams with these lengths would experience shear failure, flexural failure, and lateral-torsional buckling failure, respectively, based on the AISC 360-10 [30] design code. Eq. (1) indicates the limiting laterally unbraced length for the limit state of yielding.

$$l_p = 1.76 r_y \sqrt{E_s / F_y} \quad (1)$$

where l_p, r_y, E_s, and F_y are the minimum length of beam for occurrence of lateral-torsional buckling failure, radius of gyration along the y-axis (weak axis), Young's modulus and yield stress of steel, respectively.

The maximum allowable unbraced lengths for IPE80 and IPE100 are 533.4 mm and 630 mm, respectively. Hence, the selected 1000 mm length was long enough for steel beams to experience lateral-torsional

buckling. The total length of the steel beam was equal to the distance between the supports plus 100 mm overhang. These overhangs were provided to prevent the beams from slipping at supports. In addition, providing these overhangs were inevitable since it facilitated welding support plates. As shown in Fig. 2, welding plates at supports provided larger seating area of beams than the width of flange. This made the beam stable during the test. The support plates were not used for specimens with 1000 mm length since it could influence lateral-torsional buckling failure.

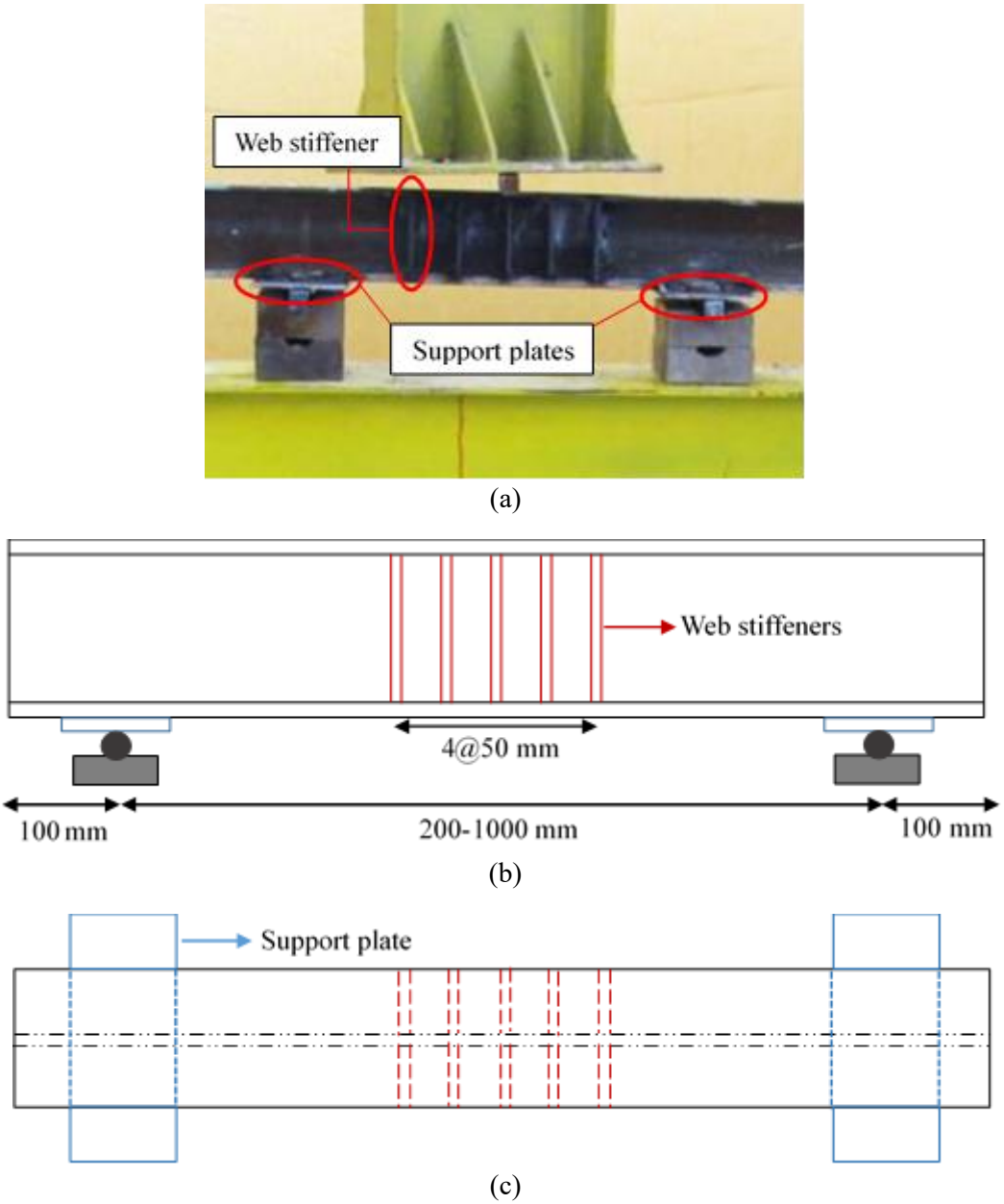

Fig. 2. (a) Support plates and web stiffeners used in the tests. (b) Side view of steel beams. (c) top view of steel beams.

The surface of CFRP laminates was cleaned with acetone, and the mounting surface of each steel beam was scrubbed by a steel wire brush in order to remove any external particles, oil, rust layers, and other bond-inhibiting materials from the surface. This provided a proper bond between steel surface and CFRP composite layer by the adhesive. The carbon laminate was placed on the adhesive layer and was hand pressed to force out air bubbles (see Fig. 3). The ends of carbon laminates experience a stress concentration during the tests [31].

Fig. 3. (a) Mixing two components of adhesive. (b) applying the epoxy adhesive on the flange surface. (c) attaching the carbon laminate to the steel beam.

Hence, after 7 days of curing of the epoxy, two ends of the carbon plate were tightly wrapped around steel beam by glass fiber-reinforced polymer (GFRP) to prevent slippage of laminates from the steel surface when loaded. The thickness of epoxy adhesive between CFRP laminate and steel beam was maintained equal to 2 ± 0.1 mm which was adequate to prevent separation between CFRP laminate and epoxy, and also between steel plate and epoxy.

For the specimens number 10, 11, 13, and 14, the CFRP laminates were attached to either one side or both sides of the beam web as shown in Fig. 4(d) and (e). In these specimens, shear strengthening method was used for steel beams designed for shear failure mode. Moreover, for flexurally strengthened specimens number 2, 3, 4, 6, 7, and 8, one layer or two layers of the CFRP laminates were attached to tension flanges or both flanges of beams (see Figs. 4(a) and (b)). In addition, the specimens number 16 and 18 were retrofitted by attaching the CFRP laminates on their compression flanges as shown in Fig. 4(c). Due to the long length of these beams, it was predicted that lateral-torsional buckling would be the

failure mode and therefore, strengthening compression flange was carried out. Moreover, as shown in Fig. 2, some web stiffeners, spaced at 50 mm, were welded to the both sides of web at midspan of beam to preclude the occurrence of web crippling.

2.3. Test setup

The beam specimens were tested using three-point bending test and seated over two cylindrical rods as simple supports (Fig. 5). The specimens were loaded monotonically by an actuator with 1000 kN load capacity. To drive the hydraulic actuator, displacement control loading was used at a constant speed of 0.06 mm/sec. This loading rate was selected to provide a reasonably continuous load-deflection curve. It should be mentioned that the mid-span displacement of steel beams was recorded by the internal linear variable differential transformer (LVDT) existed in the loading actuator.

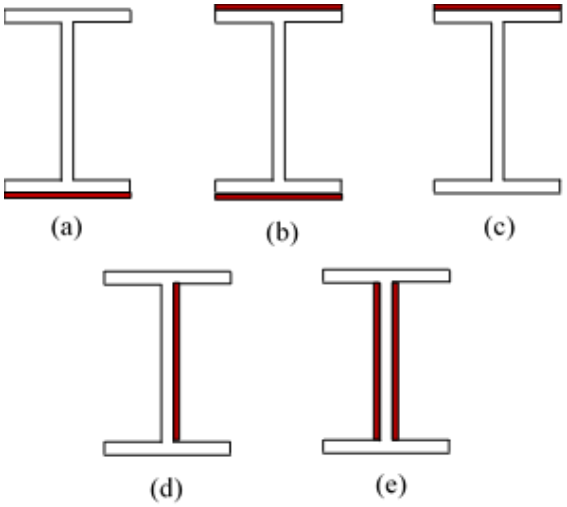

Fig. 4. Schematic configuration of strengthened specimens: attaching the carbon laminate to the (a) bottom flange, (b) both flanges, (c) top flange, (d) one side of web, and (e) both sides of web of steel beams.

3. Analytical calculations

The adhesive layer causes the CFRP strips and steel beam to act as a composite system. If the adhesive layer experiences any failure, the connection between beam and CFRP will be lost and both of them will resist the load separately. To determine the behavior of retrofitted beams, the transformed section approach [32], has been implemented in this study.

This approach provides accurate results mainly for single layer strengthening of specimens in linear elastic range. Previously presented tables 2 to 4, reveal all the pertinent mechanical properties of materials used in analytical calculation.

Three following fundamental assumptions as proposed by [32], are considered:

1) CFRP, steel beams, and adhesive have a linear elastic strain-stress relationship and remain in their elastic range.

2) There is full bond between CFRP and steel beams. In other words, no slippage occurs at the interface.

3) The distribution of strain is linear.

This method is based on the transformation of a retrofitted section with different materials into an equivalent section with one reference material. The original section and transformed section are shown in Fig. 6. The modular ratio of specimens defined as the ratio of young's modulus of CFRP laminate to young's modulus of steel is calculated by Eq. (2).

$$n = E_c / E_S \tag{2}$$

where n, E_c, and E_S are the modular ratio, Young's modulus of CFRP and steel,

respectively. After transformation, section properties will change. Since the thickness of CFRP laminates was small, its moment of inertia is neglected in the calculation of moment of inertia.

$$y = \frac{A_s(h/2)}{A_s + nA_c} \quad (3)$$

$$I = I_S + A_s(\frac{h}{2} - y)^2 + nA_c y^2 \quad (4)$$

where, y is position of neutral axis, I is moment of inertia of transformed section, h is steel beam depth, and is moment of inertia of steel section. and are the cross-sectional area of CFRP laminate and steel section, respectively.

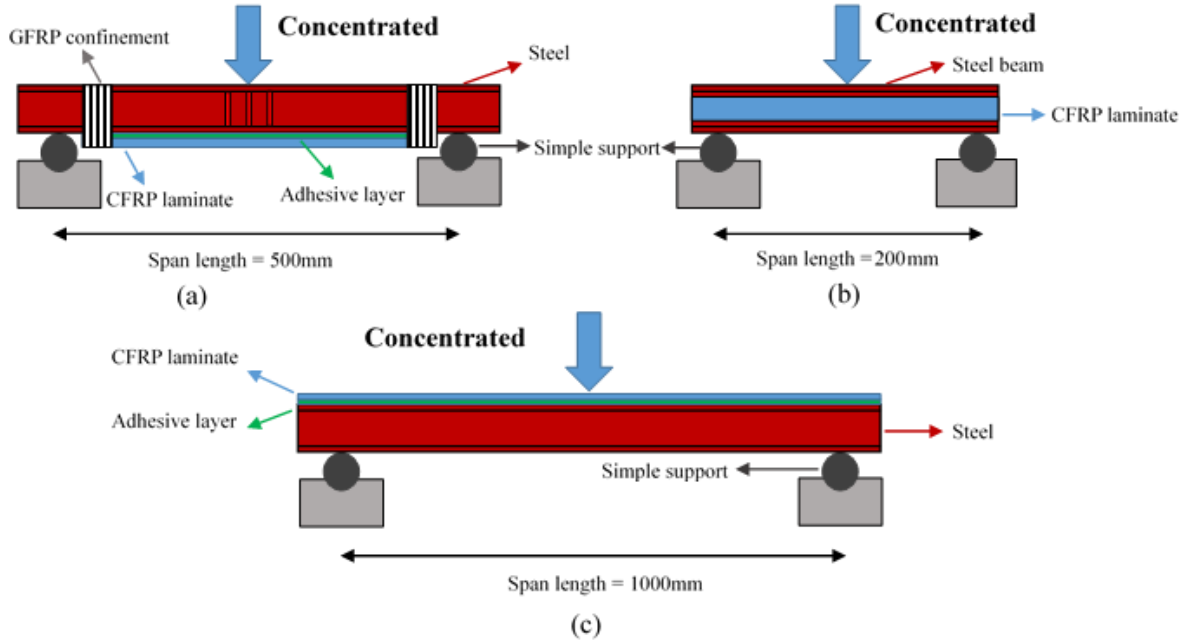

Fig. 5. Three-point bending test set-up for specimens with (a) flexural failure, (b) shear failure, and (c) lateral-torsional failure.

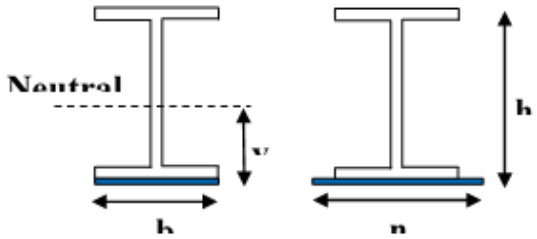

Fig. 6. The real and transformed sections.

The normal stresses in composite layer can be determined in each section along the length of beam by the following equation:

$$\sigma_c(x) = \frac{npx}{2I} y \quad (5)$$

where $\sigma_c(x)$ is the normal stress in any section with the distance of x from the beam support and p is the load applied at the mid-span.

The yield load capacity of steel beam with the flexural failure mode can be obtained by Eq. (6).

$$p_y = \frac{4F_y w_s}{l} \quad (6)$$

where p_y is the yield load capacity of steel, w_s is the section modulus of transformed section and l is the span length of beam.

4. Finite element (FE) modeling

Since the exact elastoplastic behavior of steel beams strengthened by CFRP laminates cannot be determined by the transformed section method, a finite element model was developed. In this paper, the finite element models were created using ABAQUS/CAE 6.9 [33] to simulate experimental results and also evaluate the effect of CFRP strengthening on the behavior of steel beams with different failure modes. To assess the flexural and shear behavior of the tested beams, the finite element models exactly duplicated the corresponding experimental specimens, whose section properties are given in Table 4.

Two materials, namely CFRP and steel, which were used in finite element modeling have identical properties to tested materials defined in section two. As a matter of fact, the steel was adopted as an isotropic bilinear elastoplastic material and a linear elastic stress-strain relationship was considered for CFRP laminate, respectively. As shown in Fig. 7, the strain hardening of steel after the yield point was modeled using a much lower slope than the initial slope of stress-strain diagram of material according to the test results from yield point up to ultimate stress.

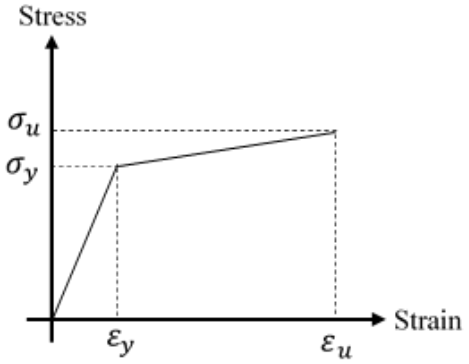

Fig. 7. Stress-strain diagram of steel used in FE model.

The first order quadrilateral shell elements with reduced integration (S4R) were used for modeling steel beams and carbon laminates. In this study, after carrying out the sensitivity analysis, a converged mesh size of 10 mm was chosen for steel beams and CFRP laminates. A sensitivity analysis was conducted using specimen F-IPE100-B (strengthened steel beam with flexural failure mode). Four different mesh sizes were chosen such that there were 30, 40, 50, and 60 elements per line along the longitudinal axis of beams, and the resulting discrepancy corresponding to these mesh sizes were 18.1, 6.0, 4.3, and 3.7 percent, respectively (see Fig. 8). Although the obtained discrepancy for model with 60 elements per line was slightly better than that for model with 50 elements per line (mesh length of 10 mm), both were acceptable while the computational cost of model with 50 elements per line was noticeably lower. The load-displacement behavior of steel beams modeled with a mesh size of 10 mm agreed well with that of tested beams, as shown in Section 6 (see Fig. 20).

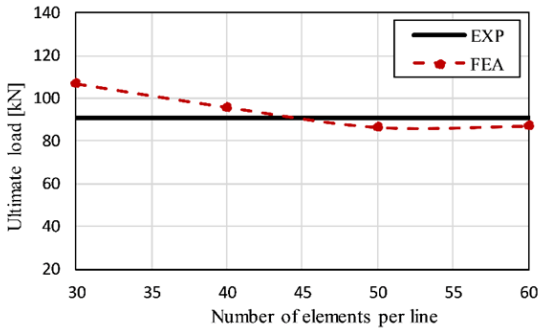

Fig. 8. Sensitivity analysis outcomes.

The adhesive layer was modeled using the spring connector elements. The translation cartesian connectors CONN2D2 which represent two-dimensional two-node connectors in ABAQUS were used as

connector elements. This method was applied in previous studies [34, 35]. The springs were arranged between two coincident meshes as shown in Fig. 9. Hence, it is indispensable to have coincident nodes above and below of adhesive layer such that those nodes are vertically connected and it makes the calculation of spring stiffness easy. In Fig. 9, the K11 and K22 are the relative elastic stiffness of the connector in the x-axis direction and y-axis direction and are calculated by the following equations:

$$K_{11} = GA/l \tag{7}$$

$$K_{22} = EA/l \tag{8}$$

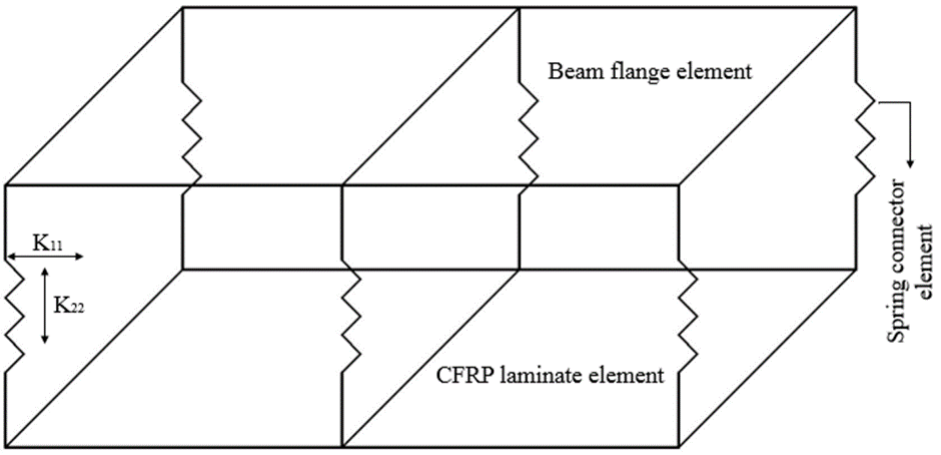

Fig. 9. Modeling of adhesive layer with spring connector elements.

Where E, G, and l are young's modulus of elasticity, shear modulus of elasticity, and thickness of adhesive, respectively. The values of young's modulus and shear modulus of epoxy adhesive used in this study were 3.5 GPa and 1.35 GPa, respectively, according to the manufacturer's catalogue and based on ASTM D638 [36] and ASTM D732 [37]. Also, the thickness of adhesive was considered equal to 2 mm.

Two reference points were created at the two ends of the steel beams and all degrees of freedom at both beam ends were tied to reference points using rigid body constraints. Then, the boundary conditions (simple and roller supports) were assigned to the two reference points.

In order to trigger the lateral-torsional buckling for specimens with 1000 mm length, a certain amount of eccentricity was considered. In fact, an initial torsional moment was generated by this eccentricity leading to second-order effects and triggers the lateral-torsional buckling failure. An initial imperfection of e=1 mm was applied herein, as suggested by Nguyen et al. [38]. They concluded that all of the imperfections can be modeled by introducing an initial imperfection of L /1000, in which L is the span length of steel beam, in the finite element model.

5. Test results and discussion

The test results are categorized based on the three major failures including flexural, shear, and lateral-torsional buckling modes. Displacement ductility index (DDI) and energy absorption capacity of steel beams

are two significant factors that should be considered in the design of structures under the action of earthquakes. DDI is expressed as the ratio of ultimate displacement to yield displacement of a structural member as indicated in Eq. 9.

$$DDI = \Delta_u / \Delta_y \quad (9)$$

where Δ_u and Δ_y represent the ultimate and yield displacement of steel beams, respectively. To obtained the yield displacement from the load-displacement diagram, different approaches have been presented and employed in the literature [39-41]. According to one of these methods, two tangent lines passing the linear part of curve and peak load point of the diagram are drawn, respectively. As shown in Fig. 10, the point of intersection of these two lines is designated H. Then a vertical line is drawn from point H to intersect the curve at point I. Finally, a secant line passing points O and I intersects the tangent line passing the peak load point at point A. the displacement value of point A is considered as the yield displacement value [41].

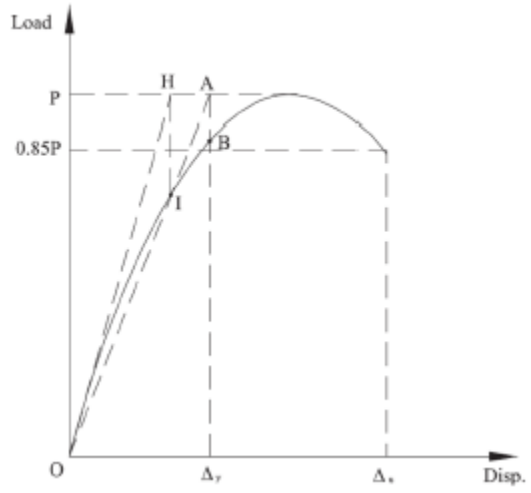

Fig. 10. Procedure to calculate yield displacement [41].

Moreover, the enclosed area under load-displacement curve is defined as the ability of specimen to absorb energy [42, 43] (see Fig. 11). Hence, the value of energy absorption capacity of specimens can be calculated using Eq. 10.

$$\text{Absorbed energy} = \int_0^{\Delta_u} P d\Delta \quad (10)$$

in which P is equal to the value of applied load. The calculate values of DDI and energy absorption capacity of each set of specimens are given in Tables 6-9.

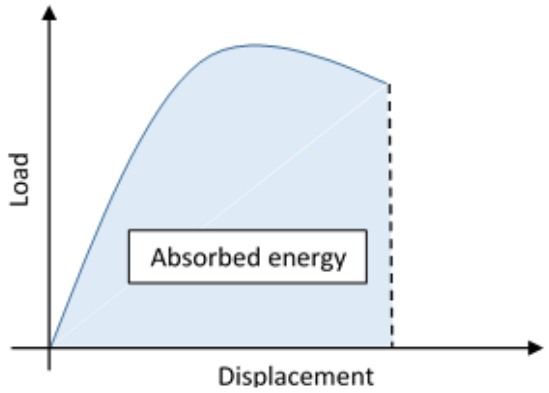

Fig. 11. Procedure to calculate energy absorption capacity of beams.

5.1. Beams with flexural failure mode

The load-deflection diagrams of control and strengthened specimens are presented in Fig. 12. The major results are given in Table 6. The specimens were loaded until the mid-span deflection reached 25 mm. The load carrying capacity of beams was compared with that at the deflection of 4 mm as well. This deflection corresponds to deflection of 1/125 beam span length. It should be noted that ultimate load capacity occurred at the deflection of 3.75/125 to 5/125 beam span length (i.e., 15 to 20 mm).

5.1.1. Strengthened beam using one layer of CFRP laminate at the bottom flange

The strengthened and control specimens diagrams are linear up to yield points and then the slope of load-displacement curve decreases and presents plastic behavior. The yield load of specimens F-IPE80-B and F-IPE100-B were increased by 9.85 and 4.75 percent in comparison to their corresponding control specimens, respectively. However, the strengthened and control beams experienced yielding at approximately the same mid-span deflections. The yield load of these specimens was computed analytically, based on the transformed section method and compared with the test results as given in Table 7. The maximum difference between experimental and analytical yield load is 7 percent. Also, the finite element modeling reports the yielding load satisfactorily with a maximum difference of 3 percent.

Table 6. Test results of specimens with flexural failure mode.

Specimen	Yield load (kN)	Ratio of yield load to control	Ultimate load capacity (kN)	Ratio of ultimate load capacity to control	Load at 4 mm deflection (kN)	Ratio of load at 4 mm deflection to control	Absorbed energy (kN.mm)	DDI
F-IPE80-C	39.18	1	48.19	1	44.91	1	1274.49	13.16
F-IPE80-B	43.04	1.10	57.44	1.19	50.58	1.13	1519.59	14.88
F-IPE80-BB	44.87	1.15	62.38	1.29	54.82	1.22	1634.47	15.34
F-IPE80-TB	43.52	1.11	58.84	1.22	53.38	1.18	1572.30	16.78
F-IPE100-C	67.16	1	77.02	1	72.30	1	1952.25	12.89
F-IPE100-B	70.35	1.05	90.48	1.17	79.16	1.09	2198.02	14.53
F-IPE100-BB	76.15	1.13	97.70	1.26	87.39	1.20	2403.65	14.97
F-IPE100-TB	72.42	1.08	91.45	1.18	81.14	1.12	2291.69	15.92

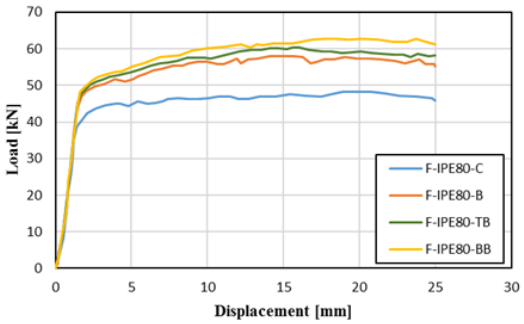

(a)

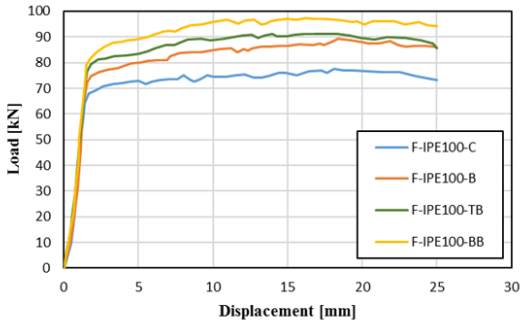

(b)

Fig. 12. The load-deflection behavior of control and reinforced flexural specimens of (a) IPE80 and (b) IPE100.

The test data indicates that the load carrying capacity at deflection of 4 mm and ultimate load carrying capacity for specimen F-IPE80-B increased by 12.62 and 19.19 percent, respectively. Table 6 reveals that the load carrying capacity at deflection of 4 mm and ultimate load carrying capacity for specimen F-IPE100-B increased by 9.48 and 17.47 percent, respectively. Furthermore, the absorbed energy of strengthened steel beams, namely F-IPE80-B and F-IPE100-B, augmented by 19.23 and 12.58 percent, when compared to control specimens, respectively. During the experiment, none of the laminates fiber experienced tensile failure and no delamination occurred.

5.1.2. Strengthened beam using two layers of CFRP laminate at the bottom flange

The test results of specimens F-IPE80-BB and F-IPE100-BB are presented by the load

versus displacement diagram in Figs. 12 (a) and (b), respectively. As Fig. 12 shows, the flexural behavior of strengthened specimens are linear up to yield points and thereafter the slope of curves decreases and shows plastic behavior. The test results indicate that the yield load of specimens F-IPE80-BB and F-IPE100-BB augmented by 14.52 and 13.38 percent in comparison to control specimens, namely F-IPE80-C and F-IPE100-C, respectively. However, the yielding of the strengthened and control specimens occurred approximately at same mid-span deflections. The yield loads of these specimens were determined by analytical calculation, based on the transformed section method and compared with their corresponding test results as given in Table 7. The maximum difference between the yield load obtained experimentally and analytically is 10 percent, while this difference between experimental and FE results is 8 percent.

Table 7. Comparison between experimental and analytical and numerical calculations for flexural failure mode.

Specimen	Yield load, Exp (kN)	Yield load, analytical (kN)	Ratio of yield load, Exp/analytical	Yield load, FE model (kN)	Ratio of yield load, Exp/FE	Ultimate load capacity, Exp (kN)	Ultimate load capacity, FE mode (kN)	Ratio of ultimate load capacity, Exp/FE
F-IPE80-C	39.18	38.40	1.02	37.98	1.03	48.19	46.68	1.03
F-IPE80-B	43.04	40.12	1.07	41.86	1.03	57.44	54.88	1.05
F-IPE80-BB	44.87	41.36	1.08	42.64	1.05	62.38	59.8	1.04
F-IPE80-TB	43.52	-	-	42.1	1.03	58.84	56.38	1.04
F-IPE100-C	67.16	65.66	1.02	65.03	1.03	77.02	74.22	1.04
F-IPE100-B	70.35	67.69	1.04	68.79	1.02	90.48	86.57	1.05
F-IPE100-BB	76.15	69.42	1.10	70.36	1.08	97.70	93.14	1.06
F-IPE100-TB	72.42	-	-	69.45	1.04	91.45	86.83	1.05

The test results reveal that the load carrying capacity of specimen F-IPE80-BB and F-IPE100-BB at deflection of 4 mm significantly increased by 22.06 and 20.87 percent in comparison to specimens F-IPE80-C and F-IPE100-C, respectively. The ultimate load bearing capacity of the strengthened beams, namely F-IPE80-BB and F-IPE100-BB, were 29.44 and 26.85 percent more than their control beams. Additionally, the energy absorption of retrofitted specimens F-IPE80-BB and F-IPE100-BB was 28.25 and 23.12 percent more than their control specimens, respectively. During the experiments, no delamination of the CFRP laminates was observed.

5.1.3. Strengthened beam using two layers of CFRP laminate one at the top and one at the bottom flange

Fig. 12 Shows the load-displacement curve of specimens F-IPE80-TB and F-IPE100-TB. Although for both specimens the yield load occurred approximately at almost similar deflections in comparison to control specimens, the strengthened beams experienced an enhancement of 11.07 and 7.83 percent in their yield load capacity. The maximum difference between experimental and finite element yield load is 4 percent. The load carrying capacity at deflection of 4 mm and the ultimate load capacity of specimen F-IPE80-TB showed a significant increase of 18.85 and 22.10 percent in

comparison to control specimen, respectively. The load carrying capacity at the mid-span deflection of 4 mm and the ultimate load capacity of specimen F-IPE100-TB increased 12.22 and 18.73 percent more than the control beam, respectively. Besides, the absorbed energy of the strengthened beams, namely F-IPE80-TB and F-IPE100-TB, was increased by about 23.37 and 17.38 percent, respectively. During the test, no delamination of the bottom CFRP laminate was recorded. Also, the top CFRP laminate in the strengthened specimens of F-IPE80-TB and F-IPE100-TB experienced laminate buckling shortly after debonding due to its small moment of inertia about the weak axis. Therefore, laminate buckling occurred at mid-span of these specimens, where the compressive normal stress is maximum.

Table 8. Test results of beams with shear failure mode.

Specimen	Ultimate load capacity (kN)	Ratio of ultimate load capacity to control	Ultimate load capacity, FE model (kN)	Ratio of ultimate load, Exp/FE	Absorbed energy (kN.mm)	DDI
S-IPE80-C	90.05	1	88.16	1.02	166.33	7.87
S-IPE80-R	99.45	1.10	95.60	1.04	181.83	8.03
S-IPE80-RL	102.43	1.14	98.29	1.04	189.27	8.26
S-IPE100-C	125.92	1	123.03	1.02	238.01	7.75
S-IPE100-R	135.18	1.07	131.03	1.03	252.52	7.87
S-IPE100-RL	140.27	1.11	135.01	1.04	265.51	8.10

5.2. Beams with shear failure mode

The load-displacement curves in Figs. 13 (a) and (b) present the test results of specimens with shear failure mode. The major data of experiments are given in Table 8. The CFRP laminates used for shear strengthening were implemented on one side (S-IPE80-R and S-IPE100-R) or both sides (S-IPE80-RL and S-IPE100-RL) of beam web. The direction of fibers was oriented in the same direction with the longitudinal axis of steel beams. However, it is not the best direction for the orientation of CFRP laminates since the maximum tensile stress in web is inclined and has an angel with CFRP direction. Hence, it is best to use bi-directional CFRP laminate in case of shear strengthening.

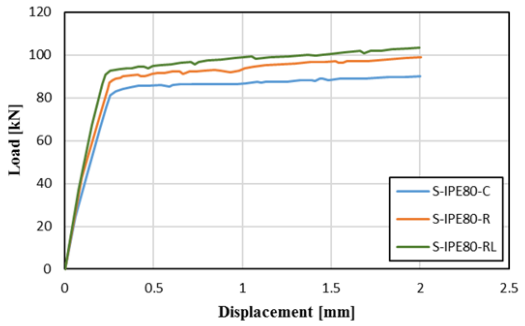

(a)

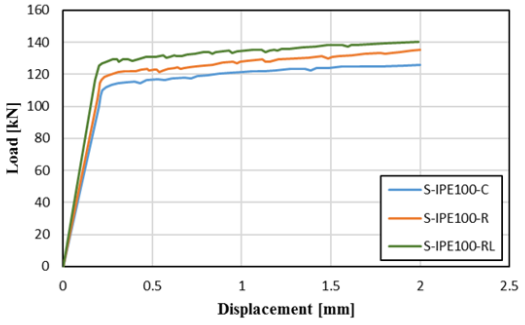

(b)

Fig. 13. Load-deflection behavior of control and strengthened shear specimens of (a) IPE80 and (b) IPE 100.

5.2.1. Strengthened beam using one layer of CFRP laminate on one side of beam web

As Figs. 13 (a) and (b) show, the response of strengthened and control specimens is almost bilinear with 10.44 and 7.35 percent increase in ultimate load capacity due to the presence of CFRP laminate for S-IPE80-R and S-IPE100-R, respectively.

The absorbed energy of CFRP specimens is 9.32 and 6.10 percent more than control steel beams. The partial debonding of CFRP occurred at the top and bottom of web and near the support of beam S-IPE80-R (Fig. 14), whereas the beam S-IPE100-R failed by CFRP parallel cleavages oriented at almost 45 degrees as shown in Fig. 15.

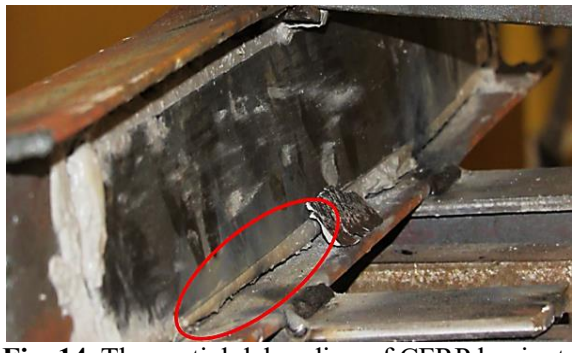

Fig. 14. The partial debonding of CFRP laminate from the surface of steel web in beam S-IPE80-R.

Fig. 15. CFRP parallel cleavages oriented at almost 45 degrees in beam S-IPE100-R.

5.2.2. Strengthened beam using one layer of CFRP laminate on each side of beam web

Figs. 13 (a) and (b) indicate that the load-displacement curve for both retrofitted and control specimens are linear and thereafter the slope of diagrams decrease. The strengthened beams of S-IPE80-RL and S-IPE100-RL experience 13.74 and 11.39 percent enhancement in ultimate load capacity. The absorbed energy of strengthened specimens is 13.79 and 11.55 percent more than control specimens. Also, the CFRP laminates experienced parallel cleavages with the general slope of 45 degrees from the longitudinal axis of beams.

5.3. Beams with lateral-torsional buckling failure mode

The top flange (compression flange) of 1000-millimeter-length specimens were strengthened by CFRP laminate to enhance lateral-torsional buckling resistance of steel beams. Figs. 16 (a) and (b) demonstrate load versus mid-span displacement of control and strengthened beams. The response of tested beams was linear and then the curves turned almost flat. Thereafter, the beams buckled, moved laterally, and finally became unstable. As shown in Fig. 17, all of the long-length steel beams (control and strengthened beams) experienced lateral-torsional buckling. The stress at compression part of beam section was diminished since the CFRP plates were attached to the top flange of retrofitted specimens. Hence, the strengthened steel beams experienced lateral-torsional buckling failure mode at higher load.

To provide safe condition, loading was stopped at mid-span deflection of 4.5 mm. The most important data of test results are reported in Table 9. The ultimate load

carrying capacity of specimens LT-IPE80-T and LT-IPE100-T was 10.06 and 7.78 percent more than the reference beams, respectively. Moreover, the amount of absorbed energy of strengthened beams LT-IPE80-T and LT-IPE100-T was 7.31 and 4.27 percent more than control beams.

Table 9. Test results of beams with lateral-torsional buckling failure mode.

Specimen	Ultimate load capacity (kN)	Ratio of strength ultimate load capacity	Ultimate load capacity using FE model (kN)	Ratio of ultimate load, Exp/FE	Absorbed energy (kN.mm)
LT-IPE80-C	22.35	1	21.28	1.03	60.94
LT-IPE80-T	24.60	1.10	23.84	1.03	65.40
LT-IPE100-C	46.49	1	45.37	1.02	125.79
LT-IPE100-T	50.11	1.08	48.46	1.03	131.16

Since loading was stopped at a predefined deflection to provide safe condition, DDI cannot be a meaningful parameter for these beams.

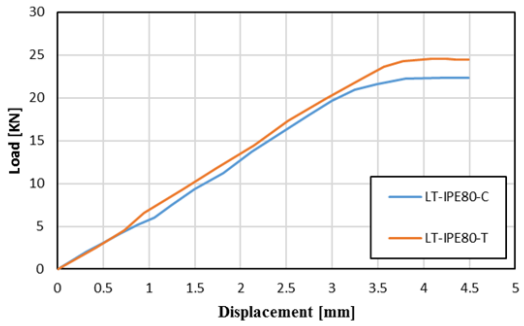

(a)

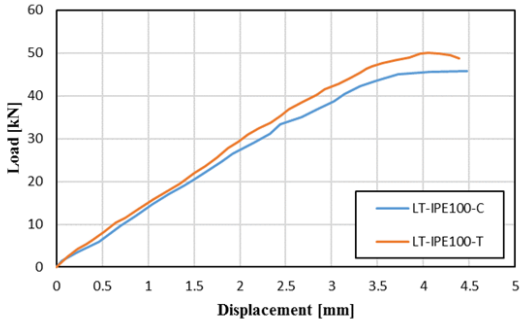

(b)

Fig. 16. The load-deflection behavior of control and strengthened specimens with lateral-torsional buckling for both (a) IPE80 and (b) IPE100.

During the experiments, two strengthened beams with CFRP laminates covering the compression flange experienced laminate buckling shortly after debonding of laminate since the moment of inertia of CFRP laminate about its weak axis was considerably low (see Fig. 18).

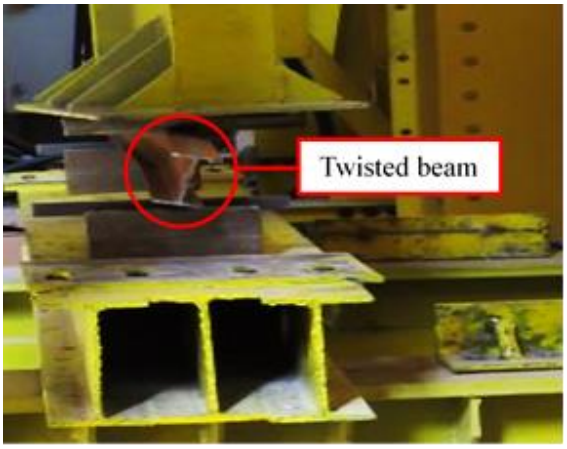

(a)

(b)

Fig. 17. (a) Twisted steel beam during the test. (b) Lateral-torsional buckling failure mode in LT-IPE100-T.

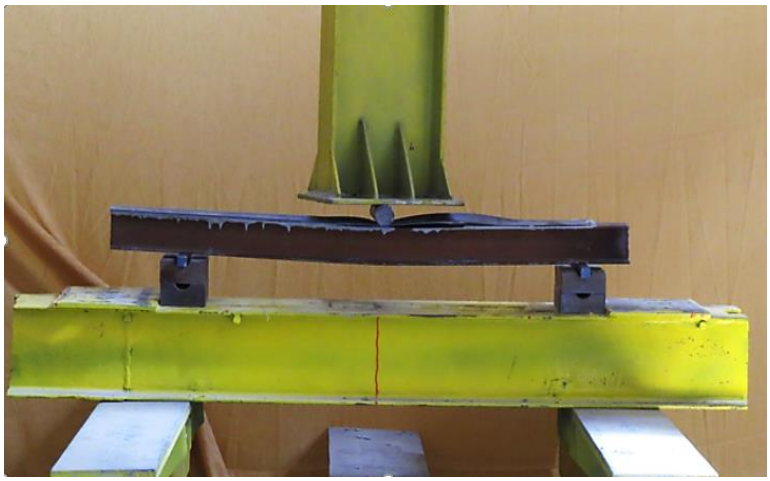

Fig. 18. Buckling of CFRP laminate covering top flange of steel beam.

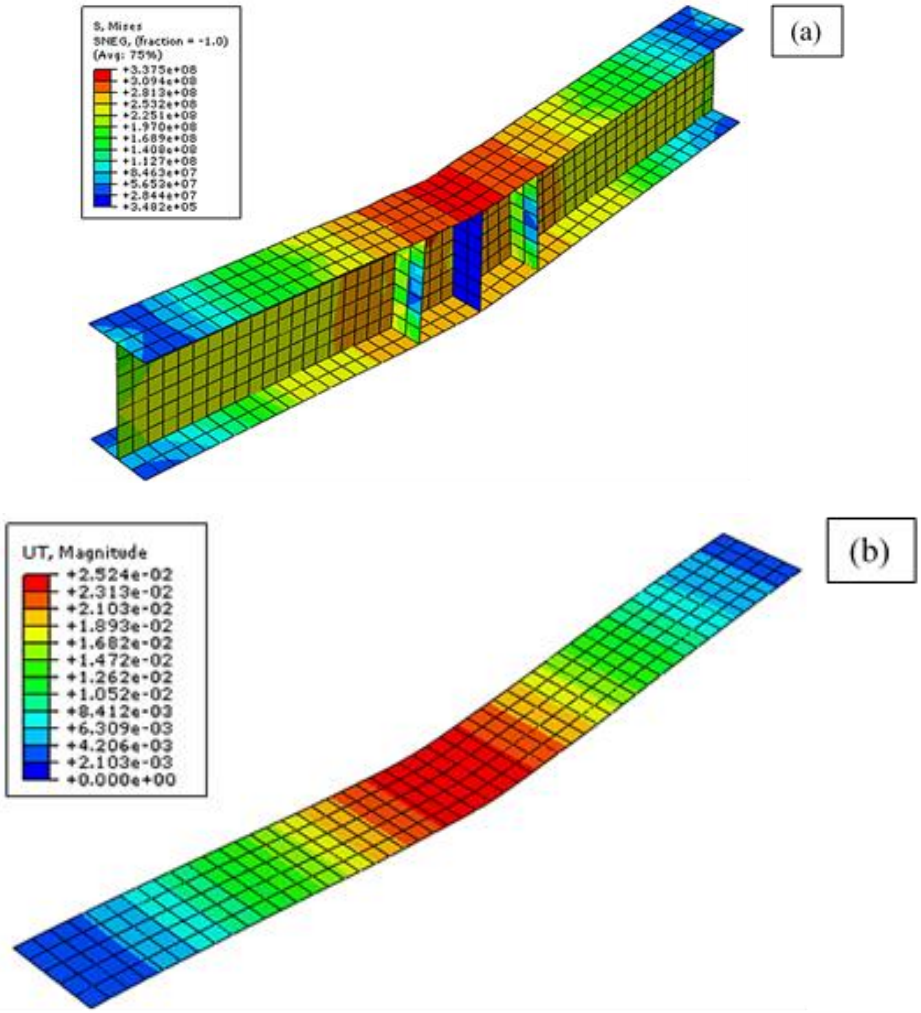

Fig. 19. Typical distribution of FE modeling at failure stage for beams (a) the Mises stress in steel beam F-IPE80-B and (b) the displacement of CFRP laminate of beam F-IPE80-B.

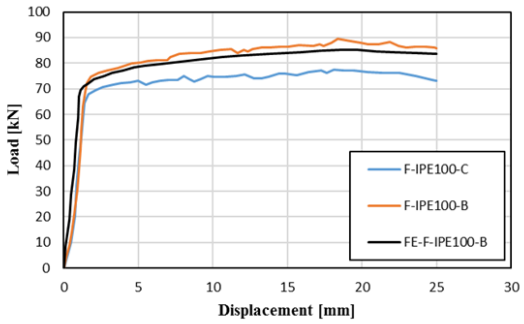

(a)

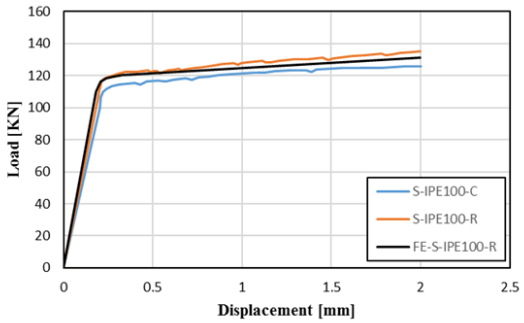

(b)

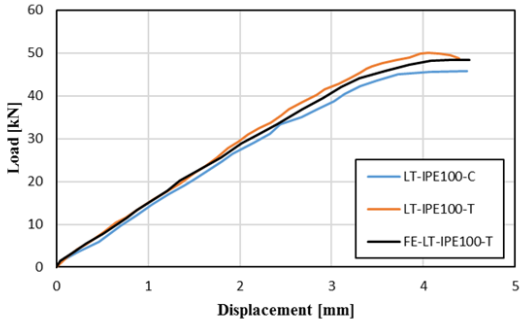

(c)

Fig. 20. Finite element results and test results of beam specimen (a) F-IPE100-B, (b) S-IPE100-R, and (c) LT-IPE100-T.

6. FE results

The finite element models for each beam specimen with various strengthening methods and control steel beams were created and analyzed using ABAQUS dynamic explicit. Fig. 19 shows a typical FE modeling at the failure stage for CFRP strengthened steel beam specimens. The distribution of mises stress in steel beam and the distribution of displacement in CFRP laminate of specimen F-IPE100-B indicate that the failure pattern is similar to the tested specimen. The yield load capacity and load at mid-span deflection of 4 mm in specimens with flexural failure mode, and ultimate load capacity and energy absorption of all beams were obtained from the finite element modeling. The FE results simulate the test data with good correlation, as are shown in Tables 7, 8, and 9. Fig. 20 compares the FE results of strengthened beams with the test results. Moreover, the test results of control steel beams are also drawn in Fig. 20 in order to facilitate the comparison of the control and strengthened specimens with the test results.

7. Conclusions

In this paper, flexural strength, shear strength, and buckling strength of steel beams, strengthened by carbon fiber-reinforced polymer laminates were investigated. Finite element modeling was performed to simulate the behavior of strengthened beams with various failures. Test variables included length and cross-sectional size of steel beam, number of CFRP layers, and location of mounting CFRP laminates depending on failure modes. Based on the results, the key conclusions are drawn as follows:

- The test results of specimens with flexural failure mode indicate that load at yield, 4 mm deflection, ultimate, and energy absorption of strengthened specimens were significantly increased up to 14.52, 22.06, 29.44, and 28.25 percent, respectively, in comparison with control beams. This improvement of energy absorption capacity

of retrofitted steel beams is desired in design of structures under the action of earthquake. Also, it is revealed that the GFRP wrapping was effective since the CFRP plates covering the tension flange of beam did not experience pre-mature debonding during the test.

• The increase in elastic stiffness of strengthened beams was not considerably more than control beams due to the small cross-sectional area of CFRP laminates even though its Young's modulus is similar to steel.

• Based on the test results, the ultimate load carrying capacity of steel beams with shear failure mode in which the unidirectional CFRP plates were attached on the web surfaces significantly improved up to 13.74 percent. Also, the energy absorption of strengthened beams with shear failure mode experienced an enhancement of up to 13.79 percent, which is considerable for specimens with this type of failure. The test results also showed that it is better to use bidirectional CFRP layers in practice in order to prevent the composites from experiencing parallel cleavages oriented at almost 45 degrees.

• The ultimate load capacity and absorbed energy of retrofitted steel beams with lateral-torsional buckling failure mode were increased up to 10.06 percent and 7.78 percent in comparison to control beams, respectively. In these specimens, the top flange (compression flange) of steel beams was strengthened by CFRP laminates. The amount of improvement in load carrying capacity for specimens with this strengthening method is higher than or similar to that for specimens strengthened with prestressed CFRP layers applied on tension flange in the literature, but the studied method herein does not need clamps and other equipment for prestressing procedure, which can diminish the cost of project in practice.

• The finite element modeling of strengthened steel beams against various failure modes simulates experimental results satisfactorily. The test and FE model results indicate that the strengthening steel beams by using bonded CFRP laminates can be considered as an effective way to rehabilitate the steel structural members with the flexural, shear and lateral-torsional buckling failure modes.

Acknowledgments

Financial support of Iran National Science Foundation (ISNF) and Center of Excellence in Structures and Earthquake Engineering are greatly appreciated. The authors are grateful to assistance of the Structural Dynamics Strong Floor Laboratory staff at Sharif University of Technology (SUT).

References

[1] Shirmardi MM, Mohammadizadeh MR. Numerical Study on the Flexural Behaviour of Concrete Beams Reinforced by GFRP Bars. Journal of Rehabilitation in Civil Engineering. 2019, 7(4):88-99. DOI: 10.22075/jrce.2018.14701.1268.

[2] Shekarchi M, Farahani EM, Yekrangnia M, Ozbakkaloglu T. Mechanical strength of CFRP and GFRP composites filled with APP fire retardant powder exposed to elevated temperature. Fire Safety Journal. 2020, 115:103178. DOI: 10.1016/j.firesaf.2020.103178.

[3] Doostmohamadi A, Vatani Oskouei A, Kheyroddin A. An Experimental Study on Effect of Concrete Type on Bond Strength of GFRP Bars. Journal of Rehabilitation in Civil Engineering. 2020, 52-70. DOI: 10.22075/jrce.2020.19922.1392.

[4] Moradi H, Khaloo AR, Shekarchi M, Kazemian A. Effect of utilizing glass fiber-reinforced polymer on flexural strengthening of RC arches. Scientia Iranica, 2019, 26(4): 2299-2309. DOI: 10.24200/SCI.2019.21512.

[5] Kargaran A, Kheyroddin A. Experimental and numerical investigation of seismic retrofitting of RC square short columns using FRP composites. European Journal of Environmental and Civil Engineering. 2020, 1-24. DOI: 10.1080/19648189.2020.1858171.

[6] Khaloo A, Moradi H, Kazemian A, Shekarchi M. Experimental investigation on the behavior of RC arches strengthened by GFRP composites. Construction and Building Materials. 2020, 235:117519. DOI: 10.1016/j.conbuildmat.2019.117519.

[7] Shekarchi M, Farahani EM, Oskouei AV. Effect of seawater on pull-out behavior of glued-in single rods set parallel to the grain of timber joints. Construction and Building Materials. 2019, 222: 342-57. DOI: 10.1016/j.conbuildmat.2019.06.140.

[8] Hamzenezhadi A, Sharbatdar M. Flexural Strengthening of Deficient Reinforced Concrete Beams with Post-Tensioned Carbon Composites Using Finite Element Modelling. Journal of Rehabilitation in Civil Engineering. 2020, 8(4): 28-46. DOI: 10.22075/jrce.2020.15707.1294.

[9] Aghabozorgi P, Khaloo A. Numerical investigation of the effects of compression GFRP reinforcement on the flexural strength and ductility of reinforced concrete beams. Journal of Concrete Structures and Materials. 2020, 5(1): 31-45.

[10] Shekarchi M, Oskouei AV, Raftery GM. Flexural behavior of timber beams strengthened with pultruded glass fiber reinforced polymer profiles. Composite Structures. 2020, 241: 112062. DOI: 10.1016/j.compstruct.2020.112062.

[11] Teng J G, Yu T, Fernando D. Strengthening of steel structures with fiber-reinforced polymer composites. Journal of Constructional Steel Research, 2012, 78: 131–143. DOI: 10.1016/j.jcsr.2012.06.011.

[12] Al-Mosawe A, Al-Mahaidi R, Zhao X L. Effect of CFRP properties, on the bond characteristics between steel and CFRP laminate under quasi-static loading. Construction and Building Materials, 2015, 98: 489–501. DOI: 10.1016/j.conbuildmat.2015.08.130.

[13] Madhavan M, Sanap V, Verma R, Selvaraj S. Flexural Strengthening of Structural Steel Angle Sections Using CFRP: Experimental Investigation. Journal of Composites for Construction, 2015, 20(1): 04015018. DOI: 10.1061/(ASCE)CC.1943-5614.0000578.

[14] Tavakkolizadeh M, Saadatmanesh H. Strengthening of steel-concrete composite girders using carbon fiber reinforced polymers sheets. Journal of Structural Engineering, 2003, 129(1): 30–40. DOI: 10.1061/(ASCE)0733-9445(2003)129:1(30).

[15] Al-saidy A H, Klaiber F W, Wipf T J. Repair of steel composite beams with carbon fiber-reinforced polymer plates. Journal of Composites for Construction, 2004, 8(2): 163–172. DOI: 10.1061/(ASCE)1090-0268(2004)8:2(163).

[16] Hmidan A, Kim Y J, Yazdani S. CFRP Repair of Steel Beams with Various Initial Crack Configurations. Journal of Composites for Construction, 2011, 15(6): 952–962. DOI: 10.1061/(ASCE)CC.1943-5614.0000223.

[17] Linghoff D, Al-Emrani M, Kliger R. Performance of steel beams strengthened with CFRP laminate - Part 1: Laboratory tests. Composites Part B: Engineering, 2010, 41(7): 509–515. DOI: 10.1016/j.compositesb.2009.05.008.

[18] Martinelli E, Hosseini A, Ghafoori E, Motavalli M. Behavior of prestressed CFRP plates bonded to steel substrate: Numerical modeling and experimental validation. Composite Structures. 2019, 207: 974-984. DOI: 10.1016/j.compstruct.2018.09.023.

[19] El Damatty A A, Abushagur M, Youssef M A. Experimental and analytical investigation of steel beams rehabilitated using GFRP sheets. Steel and Composite Structures, 2003, 3(6): 421–438. DOI: 10.12989/scs.2003.3.6.421.

[20] Lenwari A, Thepchatri T, Albrecht P. Flexural Response of Steel Beams Strengthened with Partial-Length CFRP Plates. Journal of Composites for Construction, 2005, 9(4): 296–303. DOI: 10.1061/(ASCE)1090-0268(2005)9:4(296).

[21] Rizkalla S, Dawood M, Schnerch D. Development of a carbon fiber reinforced polymer system for strengthening steel structures. Composites Part A: Applied Science and Manufacturing, 2008, 39(2): 388–397. DOI: 10.1016/j.compositesa.2007.10.009.

[22] Ghafoori E, Schumacher A, Motavalli M. Fatigue behavior of notched steel beams reinforced with bonded CFRP plates: Determination of prestressing level for crack arrest. Engineering Structures, 2012, 45: 270–283. DOI: 10.1016/j.engstruct.2012.06.047.

[23] Ghafoori E, Motavalli M. Innovative CFRP-prestressing system for strengthening metallic structures. Journal of Composites for Construction, 2015, 19(6): 04015006. DOI: 10.1061/(ASCE)CC.1943-5614.0000559.

[24] Ghafoori E, Motavalli M. Normal, high and ultra-high modulus carbon fiber-reinforced polymer laminates for bonded and un-bonded strengthening of steel beams. Materials & Design, 2015, 67: 232-243. DOI: 10.1016/j.matdes.2014.11.031.

[25] Hosseini A, Ghafoori E, Al-Mahaidi R, Zhao XL, Motavalli M. Strengthening of a 19th-century roadway metallic bridge using nonprestressed bonded and prestressed unbonded CFRP plates. Construction and Building Materials, 2019, 209: 240-259. DOI: 10.1016/j.conbuildmat.2019.03.095.

[26] Products technical information for QUANTOM® carbon plate. 2018: downloadable from http://quantom.com.tr/tr/urun/quantom-carbon-plate/

[27] ACI 440 3R-04. Guide test methods for fiber-reinforced polymers (FRPs) for reinforcing or strengthening concrete structures. American Concrete Institute, Farmington Hills, USA, 2004.

[28] Products technical information for QUANTOM® EPR 301. 2017: downloadable from http://quantom.com.tr/tr/urun/quantom-epr-301/

[29] ASTM E8 / E8M-21, Standard Test Methods for Tension Testing of Metallic Materials, ASTM

International, West Conshohocken, PA, 2021. DOI: 10.1520/E0008_E0008M-21.

[30] AISC 360-10. Specification for Structural Steel Buildings. American Institute of Steel Construction, Illinois, USA, 2010.

[31] Malek A M, Saadatmanesh H, Ehsani M R. Prediction of failure load of R/C beams strengthened with FRP plate due to stress concentration at the plate end. ACI structural Journal, 1998, 95: 142–152.

[32] Moy S S J, Nikoukar F. Flexural behaviour of steel beams reinforced with carbon fibre reinforced polymer composite. In: Proceedings of Advanced Polymer Composites for Structural Applications in Construction (ACIC 2002). Southampton: 2002.

[33] Abaqus. User's manual version 6.9. Pawtucket (RI, USA): Hibbitt, Karlsson and Sorensen lnc.; 2005.

[34] Zachariah A T. Finite Element Modelling of Adhesive Interface between Steel and CFRP. Master thesis. Chalmers University of Technology, 2006.

[35] Tahmasebi F. Finite Element Modeling of an adhesive in a bonded joint. NASA Goggard Space Flight Center, 1999.

[36] ASTM D638-10, Standard Test Method for Tensile Properties of Plastics, ASTM International, West Conshohocken, PA, 2010. DOI: 10.1520/D0638-10.

[37] ASTM D732-17, Standard Test Method for Shear Strength of Plastics by Punch Tool, ASTM International, West Conshohocken, PA, 2017. DOI: 10.1520/D0732-17.

[38] Nguyen T T, Chan T M, Mottram J T. Influence of boundary conditions and geometric imperfections on lateral–torsional buckling resistance of a pultruded FRP I-beam by FEA. Composite Structures, 2013, 100: 233-242. DOI: 10.1016/j.compstruct.2012.12.023.

[39] Dabiri H, Kheyroddin A, Kaviani A. A numerical study on the seismic response of RC wide column–beam joints. International Journal of Civil Engineering. 2019, 17(3):377-95. DOI: 10.1007/s40999-018-0364-2.

[40] Dabiri H, Kaviani A, Kheyroddin A. Influence of reinforcement on the performance of non-seismically detailed RC beam-column joints. Journal of Building Engineering. 2020, 31:101333. DOI: 10.1016/j.jobe.2020.101333.

[41] Li B, Lam ES, Wu B, Wang YY. Experimental investigation on reinforced concrete interior beam–column joints rehabilitated by ferrocement jackets. Engineering Structures. 2013, 56:897-909. DOI: 10.1016/j.engstruct.2013.05.038.

[42] Akhlaghi A, Mostofinejad D. Experimental and analytical assessment of different anchorage systems used for CFRP flexurally retrofitted exterior RC beam-column connections. Structures. 2020, 28:881-893. DOI: 10.1016/j.istruc.2020.09.037.

[43] Kheyroddin A, Dabiri H. Cyclic performance of RC beam-column joints with mechanical or forging (GPW) splices; an experimental study. Structures. 2020, 28:2562-2571. DOI: 10.1016/j.istruc.2020.10.071.